Geomorphic mapping in endorheic catchments in the Spanish Pyrenees: An integrated GIS analysis of karstic features

M. López-Vicente [*], A. Navas, J. Machín

Department of Soil and Water, Experimental Station of Aula Dei - CSIC, Avda. Montañana 1005, 50059 Zaragoza, Spain

* Corresponding author. *E-mail address:* mvicente@eead.csic.es (Manuel López-Vicente). Tel.: +34 976 716 158; fax: +34 976 716 145.

A B S T R A C T

Digital elevation models (DEMs) can be a useful tool to assess morphologically and hydrologically active processes. This paper presents a method to obtain accurate DEMs, an analysis of DEM errors and the benefits of GIS techniques for mapping geomorphological features and active processes in the karstic endorheic catchment with three permanent lakes (Estaña lakes) in the External Ranges of the Spanish Pyrenees. Field work revealed the lack of accuracy in the original DEM. A method was then proposed to obtain a hydrologically correct DEM using a Total Topographic Station (TTS) and a Global Positioning System (GPS). On a regular grid, 246 topographic points were recorded with a GPS and 237 points were measured with a TTS on areas of gentle slope. The mean and standard deviation of the error of the corrected DEM were −1.5 and 3.2 m, respectively. By using a combined flow algorithm, a flow accumulation map was derived from the corrected DEM and the study area was divided into fifteen sub-catchments. The values of the indices of watershed circularity and elongation have a strong variation and the map of flow length also showed strong asymmetry. Maps of land use, topography and lithology were created in order to establish the basis for mapping main geomorphological features. The new DEM also provided a basis for calculating the topography factor (LS) in RUSLE, an empirical soil erosion model. A map showing the error of the original DEM indicates that the highest error values occur in the main karstic features of the geomorphological map. Hence, the proposed methodology including DEM correction is useful for an accurate assessment of topographical and geomorphological features in karstic environments.

1. Introduction

An important line of research in geomorphology is to determine hydrological networks in karstic landscapes, which extend from the watershed divide down the slopes to the doline bottom. To calculate the accuracy of the geomorphological maps it is necessary to establish a methodology for an accurate assessment of hydrological networks (López-Vicente et al., 2005a). A digital elevation model (DEM) is a basis for the calculation of spatial variables that can be used in the study of ecosystems as independent estimators (Tappeiner et al., 1998) and for assessing active and passive geomorphic processes. Moreover, DEMs are sound tools to define drainage networks, as well as to provide information on the type of geomorphological evolution of the catchments in relation to their structural and lithological characteristics and the distribution of prevailing processes (Barbieri and Marchetti, 2003). One of the variables for representing active processes is the topographic factor (LS) in RUSLE, an empirical soil erosion model (Renard et al., 1997). This factor includes two components, the slope length factor (L) and the slope steepness factor (S) and they can be derived from a DEM. However, adequate DEMs are not always available. It is also known that digital elevation data and other spatial data sets are subject to inherent errors (Carlisle, 2005). Furthermore, modelling karstic areas using a DEM is more difficult than modelling normal landscapes, due to sinks in the DEM that are usually explained as errors influenced by the rounding of the elevations to the nearest integer value (Tarboton et al., 1991). In hydrogeomorphic applications it is a common practice to remove all such digital depressions in DEMs. Although this practice is inappropriate for karstic terrain where actual depressions affect many environmental phenomena, it is difficult to distinguish artefacts from actual depressions (Lindsay and Creed, 2006). Nevertheless, several studies have showed the usefulness of DEMs in characterizing karstic features (Bonnet and Colbeaux, 1999; Antonić et al., 2001).

Geographic information systems (GIS) allow the linkage of various data such as digital elevation models, results of sampling analysis, aerial photographs and geomorphological features which can be

used for geomorphological mapping (Tüfekçi and Şener, 2007). Geomorphologic characteristics of watersheds represented by quantitative descriptors such as elevation, slope, area, perimeter, mainstream length and shape (circularity ratio and basin elongation), can be automatically calculated using GIS (Apaydin et al., 2006). This paper presents the advantages of topographical and geomorphological mapping of karstic landscapes with the assistance of GIS techniques, as well as a methodology for obtaining accurate stream nets. We investigate the hypothesis that the errors in a DEM are at least partly related to the nature of the terrain (Carlisle, 2005) and examine the relationship between the DEM errors and the LS factor values.

2. Study area

The catchment of the Estaña lakes is situated in northeastern Spain (Fig. 1a) in the central part of the Pre-Pyrenees, between the Cinca and Noguera Ribagorzana Rivers, close to the northern boundary of the Ebro Basin. This study area is located between the eastern limit of the Carrodilla Range and the western limit of the Montsec Range (Fig. 1b) in a region deeply karstified with three permanent freshwater-fed lakes (Riera et al., 2006). The Pyrenees appear as an important alpine chain with a WNW-ESE direction in the western and central zones and a W-E direction in the eastern zone. The Pre-Pyrenean Mesozoic and Neogene rocks have structure of large trending folds (Martín-Serrano et al., 2005). The central part of the Pre-Pyrenees ranges is characterized by E-W trending folds forming the so-called External Ranges (Rodríguez-Fernández, 2004) reaching 900 m a.s.l. The cores of the anticlines of the External Ranges are perforated by outcrops of Triassic diapirs composed mainly of gypsiferous marls, dolostones, limestones, ophite and occasional salt deposits. The saline evaporitic deposits trigger the karstification processes with the development of dolines (Bischoff et al., 1994), some of which reach the regional water table (IGME, 1982). Regional studies have shown up the karstic nature of the areas surrounding the Estaña catchment located between the northeastern limit of the Saganta Polje (Sancho Marcén, 1988) and the western limit of the Estopiñán-Caserras Depression developed over Triassic saline materials (Martín-Serrano et al., 2005). Recently Riera et al. (2004) presented a simplified map with the main geological features of the areas surrounding the Estaña catchment, including the dolines that are associated with the lakes as well as other dolines. The

3

largest of these lakes is located at approximately 670 m a.s.l. at 42°02′N and 0°32′E. This lake is formed by two sink holes separated by a ridge which is exposed in drier periods. The maximum water depth is 22 m in the southern sink hole. The lake is mainly fed by underground springs. Nevertheless, the water level in the three lakes is partially controlled by artificial channels.

The region has a Mediterranean continental climate with two periods of intensive rainfall events, spring and autumn, and is characterized by a long summer drought. The mean annual rainfall of the study area is 595 mm, and the mean rainfall per erosive rainday in the year, defined by Renard et al. (1997), is 47.2 mm day^{-1} (Fig. 2a, b). López-Vicente et al. (2005b) analyzed rainfall data at the Benabarre, Camporrélls and Canelles weather stations for the period 1993-2004 (Fig. 1b). Rainfall values of 2005 and 2006 have been added in this study. The mean annual temperature is 12.2ºC. The coldest month is January with a mean temperature of 2.9ºC, and the hottest July with a mean temperature of 22.3ºC. Thermal inversions are frequent during the winter.

The study area is located at the transition between the Mediterranean and the Submediterranean bioclimatic regimes and presents different land covers that are dominated by evergreen oak (*Quercus rotundifolia*) with some *Buxus sempervirens*, *Juniperus oxycedrus* and submediterranean plants (Riera et al., 2006). The second plant community is dominated by dry-resistant deciduous oaks (*Quercus faginea* and *Q. cerrioides*) with some *B. sempervirens*. López-Vicente et al. (2005b) described other land covers in the study area, such as crops of winter barley and pastures and calculated the potential and real evapotranspiration for the different types of land use covers, with minimum/maximum values of 919/1249 mm and 239/425 mm, respectively.

3. Materials and methods

The methodology proposed by IGME (*Instituto Geológico y Minero de España*) for obtaining geomorphological maps (Martín-Serrano et al., 2005) links maps related to topography, hydrology, lithology and surface formations (map of geomorphic features). This procedure was adopted in this paper for mapping geomorphological features and processes after linking all the necessary information and data using ArcGIS 9.0 software.

3.1. Topography, hydrography and land use

A grid DEM (5 x 5 m, cell size) constructed by DIELMO 3D Ltd. was acquired. This DEM corresponds to the sheet 289-iii-Benabarre of the 1:25,000 Topographical Maps of Spain. The flow accumulation map was derived from the DEM by using the combined flow accumulation algorithm (MDD8) included in the HydroTools 1.0 extension developed by Holger Schäuble (www.terracs.de/Overview/overview.html). The obtained map showed many errors especially in the areas that surround the lakes and those that are located at the divides between the different sub-catchments. This first flow accumulation map unrealistically showed only one watershed as one endorheic area. A method for obtaining a correct DEM and a flow accumulation map was applied to a similar environment in the western part of the Estaña catchment (López-Vicente et al., 2005a) and showed successful results. This method includes the following steps:

(1) Derive contour lines from the grid DEM to avoid the errors associated with the main sinks. A contour interval of 3 m was selected in accordance with the cell size (5 x 5 m) of the grid DEM.

(2) Carry out field mapping in order to identify different sub-catchments and main morphological features, with the assistance of a coloured orthophoto (0.38 cm, cell size). This orthophoto was also used to determine the limits of the lakes and the locations of dolines.

(3) Carry out a field survey using a Global Positioning System (GPS) to obtain elevation data on a regular grid. In this study a grid of 100 x 100 m was used and the heights of 246 points were recorded (Fig. 3).

(4) Characterize gentle slopes and/or broad rounded ridges by using a Total Topographic Station (TTS). In the Estaña catchment, seven areas of interest including 237 elevation points were identified. The points surrounding the lakes were used as control points to compare the measured and contour-derived elevation values at each point (Fig. 3).

(5) Modify the original contour lines using all the collected information to obtain a new grid DEM.

(6) Create a flow accumulation map from the new DEM and derive the boundaries of sub-catchments.

The error map was constructed by comparing the original and the new DEMs. Moreover, two shape indices, the circularity ratio (Stepinski and Stepinski, 2005) and catchment elongation (Bàrdossy and Schmidt, 2002), were calculated for better characterizing different sub-catchments in the study area:

5

$$C = \frac{4\pi A}{P^2} \qquad (1)$$

$$E = \frac{2\sqrt{A}}{L\sqrt{\pi}} \qquad (2)$$

where C is the circularity ratio, A is the catchment area, P is the perimeter of a circle having the same area of the catchment, E is the elongation index and L is the maximum length of the catchment parallel to the principal drainage line.

A land cover map was created by using GIS and a coloured orthophoto, and eight types of cover were idenitified: urban, paths and roads, oak woodlands, Mediterranean forest, scrublands, crops, bank vegetation and pine woodlands. Finally, all the information related to the topography, hydrology and land cover was linked to obtain the land use and catchment distribution map.

3.2. Lithological map

A lithological map was made based on an existing geological map (sheet 289-Benabarre at a scale of 1:50,000, unpublished) and a field survey to better define the distribution of surface formations especially carbonates and gypsum. Soil samples were collected using the same grid system as used for the GPS measurements (Fig. 3).

3.3. Geomorphological map

A geomorphological map (strict sense) and the lithological map were linked in order to obtain a more detailed map showing the geomorphological environment. The following morphological landforms and depositional elements have been included:

(1) Structural elements: Rounded ridges, limestone scarps, gypsum diapirs, contour lines with 20 m interval and slope angles. The ridges, contour lines and slope angles were obtained from the new DEM. The ridges follow the interfluves lines included in the map of hydrology. The slope map was reclassified into two classes: gentle and medium slopes (<13º) and steeper slopes.

(2) Gravitational elements: Boulder ground and colluvial deposits.

(3) Fluvial elements: natural springs, gullies, ephemeral streams and alluvial deposits.

(4) Endorheic elements: limits of lakes and endorheic areas. The latter limits were obtained from the flow accumulation map, following the contours which define different sub-catchments.

(5) Endorheic elements: lapies, uvalas, dolines, collapsed dolines, doline deposits and bottom valley deposits.

(6) Anthropogenic elements: water canals.

Finally, the information from the maps of lithology and geomorphic features were linked in order to generate the geomorphological map.

3.4. Topography factor (LS) map

A map of morphodynamic phenomena represents information related to geomorphological processes. Such maps can be created by linking a geomorphological map and morphodynamic information (map of processes). In this paper we focus on the topography factor (*LS*) described in RUSLE as the main active morphological process related to DEMs. This factor is the product of slope length (*L*) and slope steepness (*S*). Slope length is defined as the horizontal distance from the origin of the overland flow to the point where either the slope gradient decreases enough to start deposition or runoff becomes concentrated in a defined channel (Renard et al., 1997). An increase in slope length and steepness produces high overland flow velocities and soil erosion. *L* and *S* are represented by dimensionless ratios to those for the experimental plot 22.13 m in length and 9% in slope. The physical meaning of the *LS* factor is the transport capacity of sediment by runoff.

Moore and Burch (1986a, b) proposed an equation to estimate the *LS* factor at catchment scale as a function of the contributing area ($A_{s,i}$, in m) and slope angle (α_i, in radians):

$$LS_i = \left(\frac{A_{s,i}}{22.13} \right)^{p} \left(\frac{\sin \alpha_i}{0.0896} \right)^{q} \tag{3}$$

where *p* and *q* are empirical exponents (*p* = 0.4 and *q* = 1.3; Moore and Wilson, 1992). The contributing area is calculated as the product of the flow accumulation map and the cell size of the DEM. Di Stefano et al. (2000) used this approach in the Sparacia catchment (3.64 ha) in Sicily, and in three sub-catchments (1.5, 1.4 and 1.6 ha) in the Crepacuore basin, Calabria (Italy). Martínez-Casasnovas and Sánchez-Bosch (2000) also used the approach of Moore and Burch (1986a, b) for the

steep topography of the Penedés region (province of Barcelona, Spain). The RUSLE model is only suitable for estimating erosion due to interrill and rill processes and does not account soil erosion in permanent or ephemeral streams. Hence, there is an upper limit on the slope length that should be used to modify the flow accumulation map (Renard et al., 1997). To enforce an upper limit using the above approach, the slope length was measured at 14 points that are associated with the beginning of concentrated surface flow.

4. Results and discussion

4.1. Topography, hydrography and land use

Fig. 4 shows the cell-to-cell surface flow path map derived from the new DEM following a multiple flow approach untill the number of cumulated cells reaches 500 (this threshold value was proposed by the HydroTools 1.0 extension). The map was made by choosing the direction of steepest descent to one of the eight surrounding cells. Fig. 4 also presents the endorheic limits of the fifteen sub-catchments of the Estaña catchment. Eight of them are located in the highest area in the northern part, over the same slope, four are located in the southern part, and the other three are related to the lakes. The sub-catchments of the "Estanque de Arriba" lake and the "Estanque Grande de Abajo" lake present the highest extension with an area of 74 and 120 ha, respectively. The first of these sub-catchments has the steepest slopes, with a mean value of 24.9 % (Table 1). The sub-catchments of the "Estanque Pequeño de Abajo" lake, the Doline SE and the Doline NW 1 have an area of 13, 16 and 7 ha, respectively, whereas the other sub-catchments are smaller than 5 ha. Sub-catchments above the three lakes were delineated from the new DEM. According to the flow accumulation map, the drainage pattern of the Estaña catchment can be associated with sheet flow in the upstream network and concentrated flow in the downstream gully and ephemeral-stream networks. The largest sub-catchment presents the lowest value of the circularity ratio, 0.22, whereas small sub-catchments show higher values up to 0.57 (Table 1). The mean value for the Estaña catchment is 0.35 which is typical of elongated catchments. The sub-catchments associated with the lakes have a mean elongation ratio of 1.06 whereas the rest of the sub-catchments have a mean value of 0.83.

8

The minimum and maximum values of the DEM error are -13.6 and 10.8 m, respectively (Fig. 5). The mean error ($\bar{\delta}_Z$) is -1.5 m and the standard deviation (S_Z) is 3.2 m. The percentage of area with a negative error ($< - 0.1$ m) is 63.4 %, whereas the area with negligible elevation changes (- 0.1 to 0.1 m) represent 13.3 %. The spatial-distribution of large DEM errors correspond well to the main karstic features represented in the geomorphological map. Both the highest positive and negative error values are associated with the limits of the endorheic areas and with the bottom areas of sub-catchments where dolines are located.

The different land uses shown in the topographical map (Fig. 6) have the following percentages: urban (0.1 %), paths, roads and bare soil (1.6 %), boulder grounds (0.5 %), oak woodlands (3.7 %), Mediterranean forest (41.1 %), scrublands (19.2 %), crops (mainly winter barley) and pastures (31.2 %), bank vegetation (2.3 %) and pine woodlands (0.3 %). The contour interval of the topographic map has been increased to 20 m in order to improve the readability of the map. Finally, interfluves and cells with a flow accumulation higher than 1000 are shown in the topographic map (Fig. 6).

4.2. Geomorphological map

Four different lithological units are distinguished in the new geomorphological map (Fig. 7). The first and second units correspond to Mesozoic materials including limestones and clay materials with evaporitic deposits, mainly gypsum. The third unit corresponds to colluvial deposits covering part of the northern slopes of the study area. The fourth unit corresponds to alluvial, valley-bottom and sink-hole deposits. All sub-catchments have sink-hole deposits in the lowest areas, except four sub-catchments located in the northern part of the study area, and present boulder ground materials in their inner areas.

In the geomorphological map (Fig. 7) it is necessary to highlight the broad steep area which covers 31.9% of the Estaña catchment. Seventeen dolines have been distinguished in the area, as well as two uvalas surrounding the "Estanque de Arriba" and the "Estanque Grande de Abajo" lakes. Each uvala includes two collapse dolines. Thirteen gully systems have been represented, with six of them being longer than 200 m. The hydrological features show the existence of three springs, and only one

9

ephemeral stream that starts in one of these springs does not reach the lake. Areas of gentle slopes are covered by sink-hole, alluvial and flat bottom valley deposits. There is only one typical gravitational landform, which corresponds to the colluvial deposit in the northern part of the area. The main lithological feature in this map is the outcrop of diapirs of gypsum, which covers 1.4% of the total area. Scattered boulder ground deposits appear in most sub-catchments, although they do not cover large areas in any case. Finally, lapies appear as a symbolic landform because of their limited occurrence.

4.3. Topography factor (LS) map

The upper limit of the flow length factor (L) is shown in the flow length map (Fig. 8). The mean flow length is 192 m. Since the grid cell width is 5 m, the maximum value of flow accumulation is 38.4 grid cells. Hence, the flow accumulation map was modified so that values greater than 38.4 were replaced by the value of the maximum flow accumulation. The new set of values was used to calculate the net contributing area as a parameter of Eq. (3), as well as the slope steepness per raster cell to assess the LS factor. The minimum and maximum values of the factor (Fig. 9) are 0 and 61.3, respectively, with a mean of 5.2 and a standard deviation of 4.9. The large difference between the mean and maximum values is due to the large extent of the area (86.6 %) with values lower than 10. The highest values, larger than 20, correspond to areas with the steepest slopes and presence of gullies that are mainly concentrated in the northern part of the so-called "Estanque de Arriba" and "Estanque Grande de Abajo" sub-catchments. On the other hand, pixels with a value equal to zero represent 0.14% of the study area and are located in flat areas near or within dolines, as well as near boundaries between different sub-catchments.

The topographic characteristics of the study area may explain the higher value of the upper limit of flow length, 192 m, than that estimated by Renard et al. (1997) in experimental plots, 122 m. The mean and maximum values of the LS factor estimated for the study area are quite similar to those obtained by Onori et al. (2006) in a mountainous catchment in Sicily (Italy), with mean and maximum values of 3.9 and 62.2. However, in mountains of Palestine, Hammad et al. (2004) estimated a mean value for the topographic factor of 0.36, which is lower than the mean value for the Estaña catchment.

10

Moreover, Boellstorff and Benito (2005) determined a value lower than 1.0 for the 98 % of an area in the province of Toledo (Spain). According to one of the objectives of this work, the relationship between the *LS* factor and the DEM error has been analyzed. However, it showed an insignificant correlation ($r^2 = 0.02$) based on data for 98,203 points of the study area. These results suggest that the *LS* factor is not sensitive to the accuracy of the DEM and mainly depends on slope steepness.

The geomorphological map shows the existence of active processes of erosion over the colluvial deposits and on the clay and gypsum materials as indicated by the presence of well-developed gullies. Moreover, the gully areas present high values of the *LS* factor. In four small sub-catchments in the northern part of the Estaña catchment, the leaching of fine materials has been identified at the bottom of the dolines where only boulder ground materials remain.

5. Conclusions

The methodology developed in this study is useful to find and modify errors in the DEMs, especially those associated with artefacts, actual depressions and endorheic limits. After identifying these features, it is possible to remove errors and preserve real elements in a DEM for geomorphological analysis. Such a correction of the original DEM is useful for delineating hydrological networks and other geomorphological elements in karstic areas. In spite of the weak correlation between the DEM error and the *LS* values, assessment of active geomorphic processes will be facilitated by the use of accurate DEMs for karstic landscapes. The information derived from the geomorphological and the *LS* factor maps can be used as a basis to assess areas with high, medium and low susceptibilities to erosion. The proposed methodology seems to be appropriate for application in karstic areas, but it needs to be validated for applications to other landscapes.

Acknowledgement

References

Antonić, O., Hatic, D., Pernar, R., 2001. DEM-based depth in sink as an environmental estimator. Ecological Modelling 138 (1-3), 247-254.

Apaydin, H., Ozturk, F., Merdun, H., Aziz, N.M., 2006. Determination of the drainage basin characteristics using vector GIS. Nordic Hydrology 37 (2), 129-142.

Barbieri, M., Marchetti, M., 2003. Morphometric analysis of the drainage network in the Modena and Reggio Emilia Apennines (Northern Italy) | Analisi morfometrica della rete di drenaggio nell'Appennino modenese e reggiano (Italia settentrionale). Geografia Fisica e Dinamica Quaternaria 26 (2), 87-96.

Bàrdossy, A., Schmidt, F., 2002. GIS approach to scale issues of perimeter-based shape indices for drainage basins. Hydrological Sciences-Journal-des Sciences Hydrologiques, 47(6), 931-942.

Bischoff, J.L., Julià, R., Shanks, W.S., Rosenbauer, R., 1994. Karstification without carbonic acid: bedrock dissolution by gypsum-driven dedolomitization. Geology 22, 995-998.

Boellstorff, D., Benito, G., 2005. Impacts of set-aside policy on the risk of soil erosion in central Spain. Agriculture Ecosystems & Environment 107, 231-243.

Bonnet, T., Colbeaux, J.P., 1999. Spatialized morphological analysis: A method of detecting faults, a necessity for hydrodynamics and karstologic studies of cracked aquifers. Examples of the chalky aquifers of Northern France. Geodinamica Acta 12 (3-4), 223-235.

Carlisle, B.H., 2005. Modelling the spatial distribution of DEM Error. Transactions in GIS 9 (4), 521-540.

Di Stefano, C., Ferro, V., Porto, P., 2000. Length Slope Factors for applying the Revised Universal Soil Loss Equation at Basin Scale in Southern Italy. J. Agric. Engng. Res. 75, 349-364.

Hammad, A.A., Lundekvam, H., Børresen, T., 2004. Adaptation of RUSLE in the Eastern Part of the Mediterranean Region. Environmental Management 34(6), 829-841.

IGME, 1982. Mapa Geológico de España 1:50.000. No. 289: Benabarre. Instituto Geológico y Minero de España, Madrid.

Lindsay, J.B., Creed, I.F., 2006. Distinguishing actual and artefact depressions in digital elevation data. Computers and Geosciences 32 (8), 1192-1204.

López-Vicente, M., Navas, A., 2005a. Solving topography of Digital Elevation Model in karstic environments: a case study in the External Ranges of the Pyrenees. Final Proc. Sixth International Conference on Geomorphology. Zaragoza, Spain, pp. 388.

López-Vicente, M., Nelson, R., Stockle, C.O., Navas, A., Machín, J., 2005b. Modelización de la capacidad de transporte distribuida en subcuencas endorreicas del Pirineo oscense. Final Proc. II Simposio Nacional Sobre Control de la Degradación de Suelos. Madrid, Spain, pp. 813-817.

Martín-Serrano, A., Nozal, F., Salazar, A., Suárez, A., 2005. Geomorfología subaérea. Explicación de los elementos representados. In: Martín-Serrano, A. (Ed.), Mapa Geomorfológico de España y del margen continental a escala 1:1.000.000. IGME, Madrid, pp. 23-44.

Martínez-Casasnovas, J.A., Sánchez-Bosch, I., 2000. Impact assessment of changes in land use/conservation practices on soil erosion in the Penedès–Anoia vineyard region (NE Spain). Soil & Tillage Research 57, 101-106.

Moore, I., Burch, G., 1986a. Physical basis of the length-slope factor in the universal soil loss equation. Soil Science Society of America Journal 50, 1294-1298.

Moore, I., Burch, G., 1986b. Modeling erosion and deposition: topographic effects. TRANS of ASAE 29(6), 1624-1640.

Moore, I.D., Wilson, J.P., 1992. Length-slope factors for the Revised Universal Soil Loss Equation: simplified method of estimation. Journal of Soil and Water Conservation 47(5), 423-428.

Onori, F., De Bonis, P., Grauso, S., 2006. Soil erosion prediction at the basin scale using the revised universal soil loss equation (RUSLE) in a catchment of Sicily (southern Italy). Environmental Geology 50, 1129-1140.

Renard, K.G., Foster, G.R., Weesies, G.A., McCool, D.K., Poder, D.C., 1997. Predicting Soil Erosion by Water: A Guide to Conservation Planning with the Revised Universal Soil Loss Equation (RUSLE). Handbook #703. US Department of Agriculture, Washington, DC.

Riera, S., López-Sáez, J.A., Julià, R., 2006. Lake responses to historical land use changes in northern Spain: The contribution of non-pollen palynomorphs in a multiproxy study. Review of Palaeobotany and Palynology 141, 127–137.

Riera, S., Wansard, G., Julià, R., 2004. 2000-year environmental history of a karstic lake in the Mediterranean Pre-Pyrenees: the Estanya lakes (Spain). Catena 55(3), 293-324.

Rodríguez-Fernández, L.R., 2004. Mapa Tectónico de España a escala 1:2.000.000. In: Vera, J.A., (Ed.), Geología de España. SGE-IGME, Madrid.

Sancho Marcén, C., 1988. El polje de Saganta (Sierras Exteriores Pirenaicas, Provincia de Huesca). Cuaternario y Geomorfología 2 (1-4), 107-114.

Stepinski, T. F., Stepinski, A. P., 2005. Morphology of drainage basins as an indicator of climate on early Mars. Journal of Geophysical Research 110, E12S12.

Tappeiner, U., Tasser, E., Tappeiner, G., 1998. Modelling vegetation patterns using natural and antropogenic influence factors: preliminary experience with a GIS based model applied to an Alpine are. Ecol. Model. 113, 225-237.

Tarboton, D.G., Bras, R.L., Rodriguez-Iturbe, I., 1991. On the extraction of channel networks from digital elevation data. Hydrol. Processes 5, 81-100.

Tüfekçi, K., Şener, M., 2007. Evaluating of karstification in the Menteşe Region of southwest Turkey with GIS and remote sensing applications. Zeitschrift fur Geomorphologie 51 (1), 45-61.

Table 1. Morphometric parameters of the new DEM.

Catchment		Area (ha)	Perimeter (m)	Elevation (m a.s.l.)			Slope (%)	Shape indices	
ID	Name			min	max	mean	Mean[a]	Circularity	Elongation
	Estaña catchment	245.51	9400	676.0	896.0	741.0	19.1	0.35	–
	Lakes	17.33	–	676.0	682.0	676.5	–	–	–
1	Doline NW 1	7.50	1680	817.6	862.6	830.1	12.1	0.33	0.84
2	Doline NW 2	1.00	540	841.9	869.2	851.0	21.3	0.43	0.92
3	Doline NW 3	2.04	720	858.6	896.0	874.8	21.3	0.49	0.86
4	Doline boulder 1	0.45	360	842.0	860.2	849.6	15.3	0.44	0.64
5	Doline boulder 2	0.07	120	832.0	837.2	834.1	16.9	0.57	1.19
6	Doline boulder 3	0.13	190	829.8	833.6	831.1	8.7	0.44	1.10
7	Doline NE 1	3.57	970	841.3	890.0	853.3	20.7	0.48	0.87
8	Doline NE 2	2.08	760	808.8	841.9	822.5	23.4	0.45	0.83
9	"Estanque de Arriba" lake	74.49	5300	679.0	892.2	753.5	24.9	0.33	0.94
		72.82[a]							
10	"Estanque Grande de Abajo" lake	120.05	8200	676.0	871.6	720.2	16.8	0.22	0.87
		104.86[a]							
11	"Estanque Pequeño de Abajo" lake	13.43	1800	682.0	725.0	695.4	15.0	0.52	1.37
		2.96[a]							
12	Doline E	2.78	940	731.1	755.0	739.7	10.6	0.39	0.63
13	Doline SE	16.38	2400	683.9	746.0	707.5	15.4	0.36	0.74
14	Doline SW 1	1.33	680	685.9	711.0	693.3	18.0	0.36	0.63
15	Doline SW 2	0.25	300	697.6	710.3	701.8	13.8	0.34	0.69

[a] Without accounting the area of the lakes.

Fig. 1. The study area. (a) Location of the study area in the province of Huesca (Spain). (b) Detailed map and the locations of the weather stations in the External Ranges of the Pyrenees.
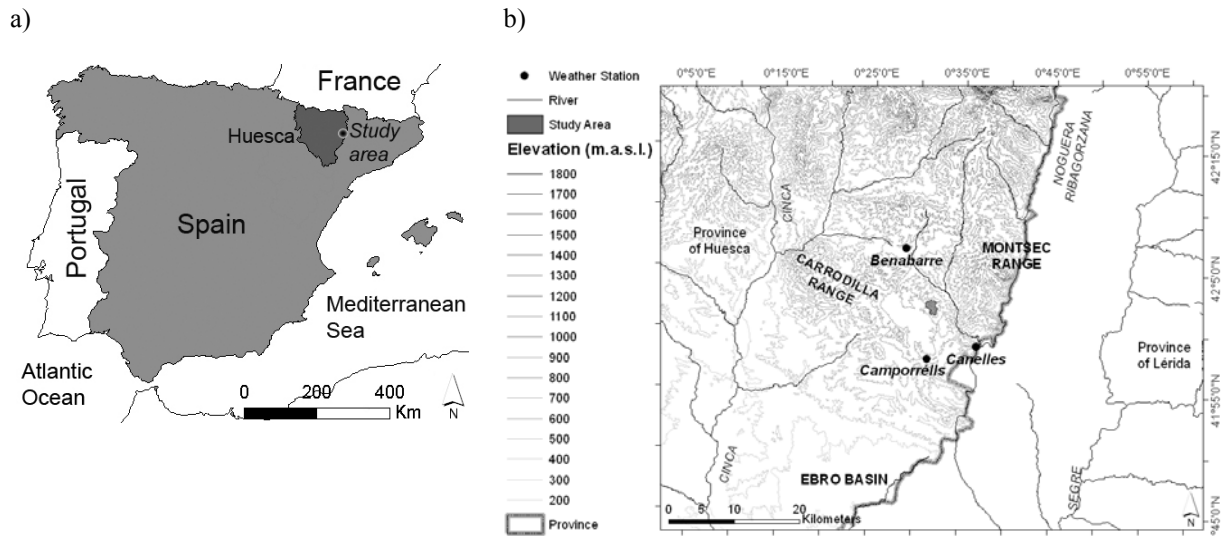
a)

b)

Fig. 2. Climate of the study area. (a) Mean monthly rainfall (R) and minimum (Tmin) and maximum (Tmax) temperatures. (b) Number of monthly rainfall events and number and percentage of monthly erosive rainfall events.
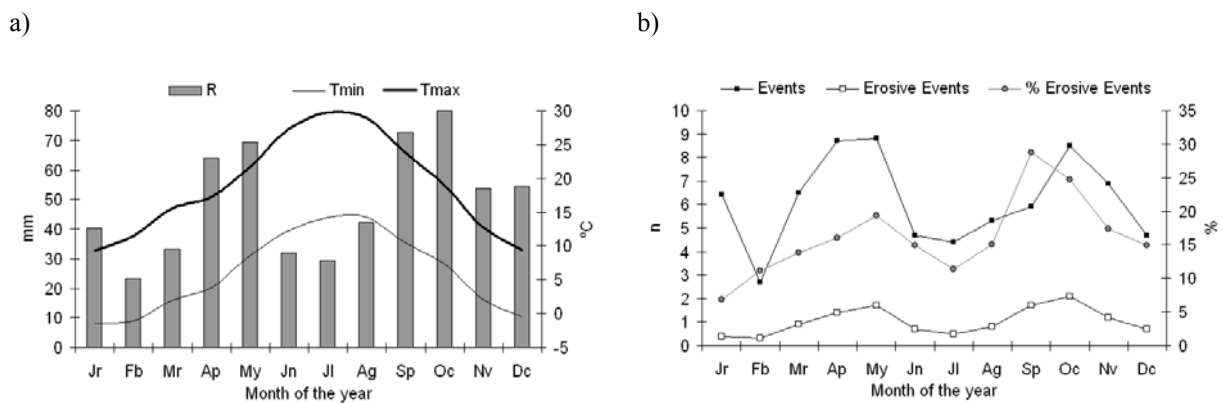
a)

b)

Fig. 3. Measurement points of elevation with GPS and TTS, and modified contour lines with 3 m interval.
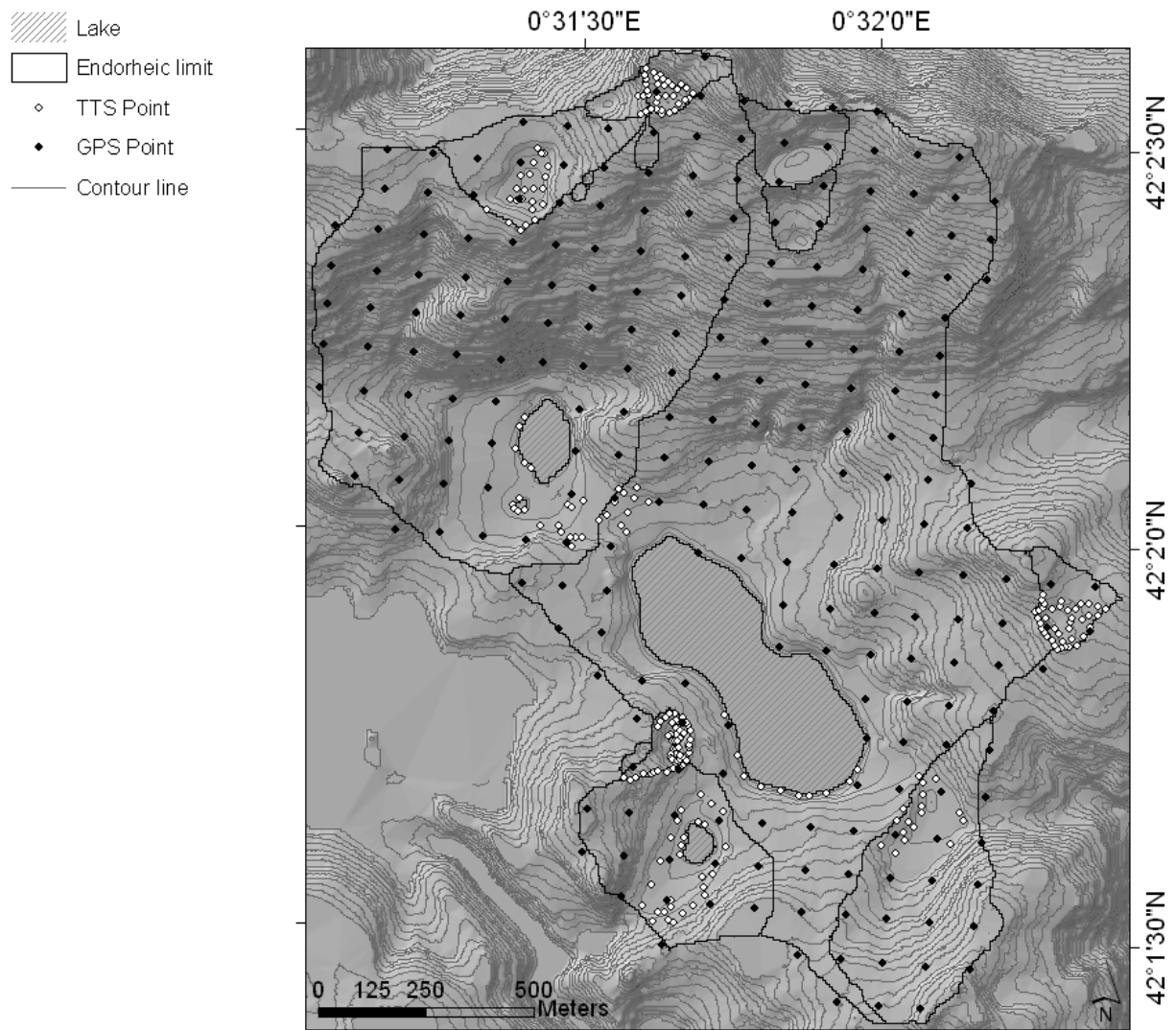
Fig. 4. Interfluves and flow accumulation map derived from the new DEM.
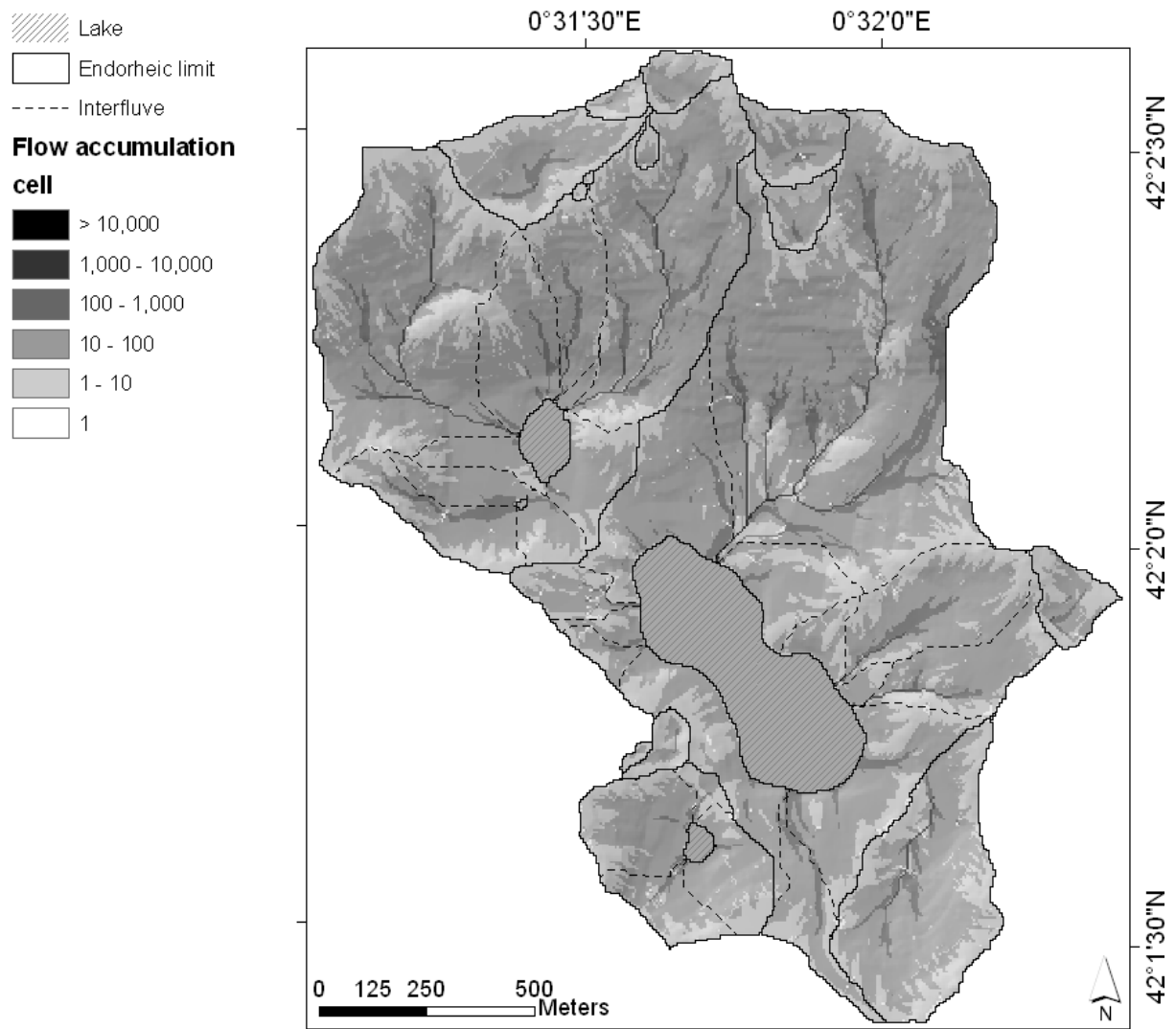
Fig. 5. Map of error values of the original DEM.
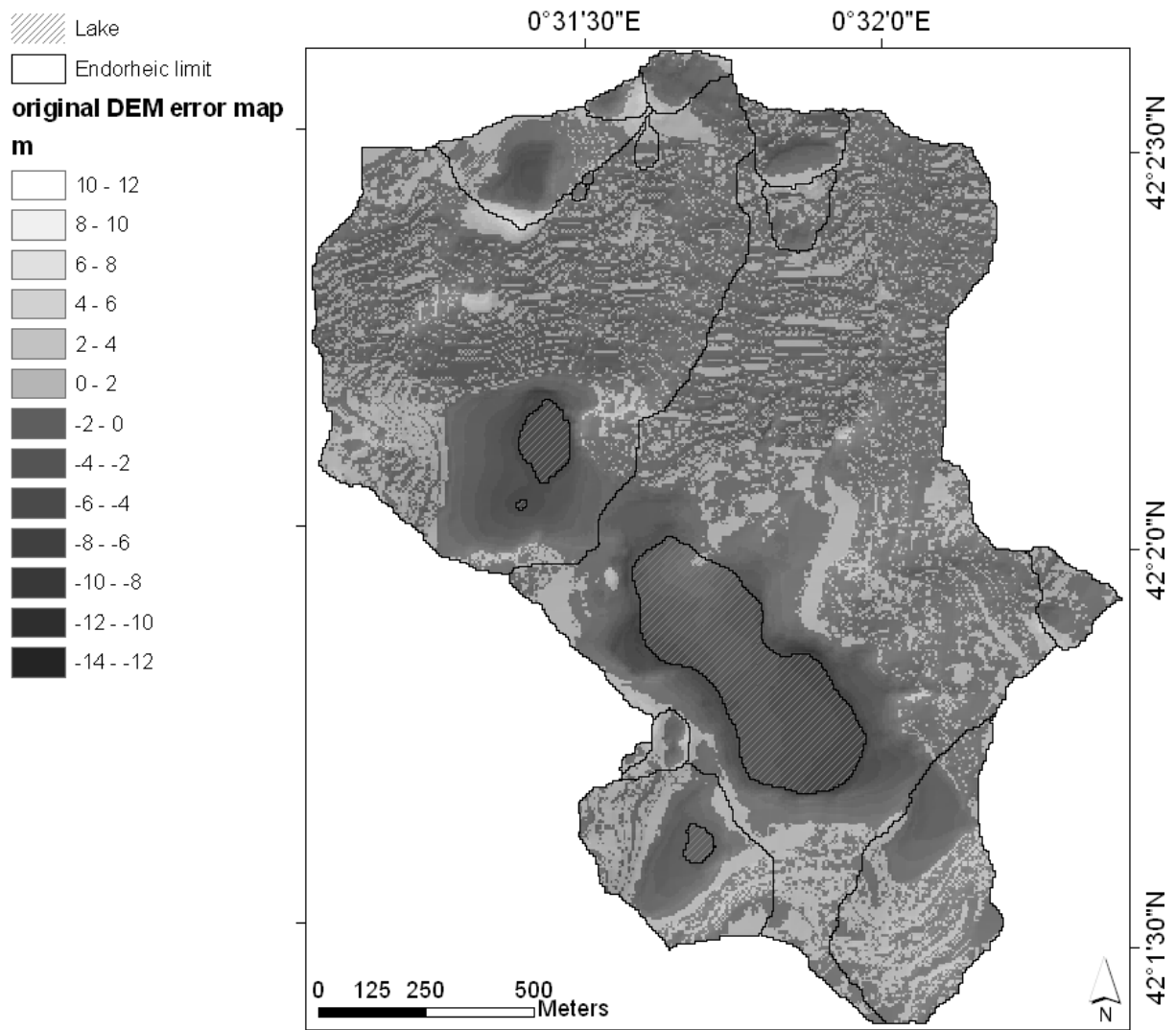
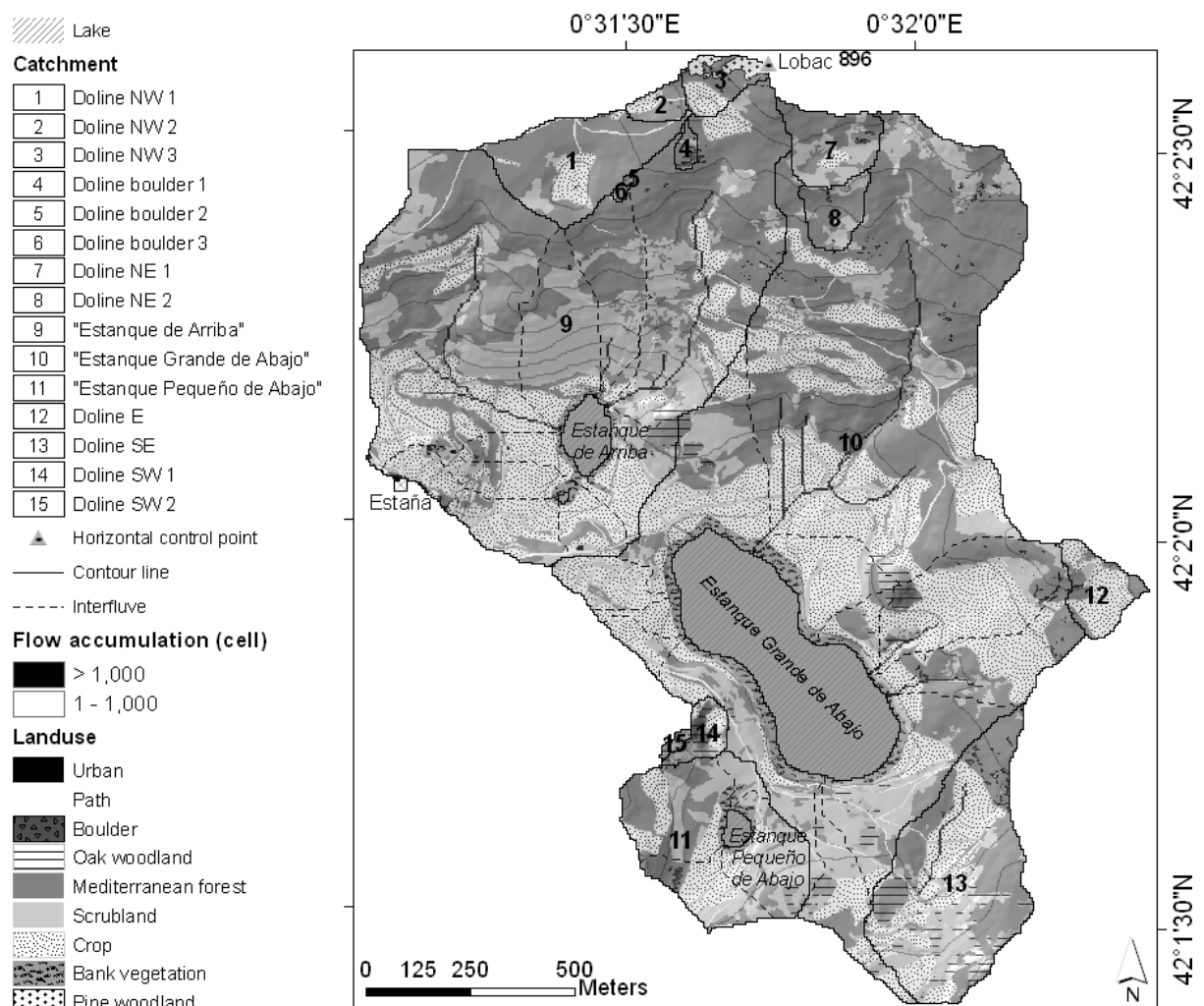**Fig. 6.** Land use and catchment distribution map.
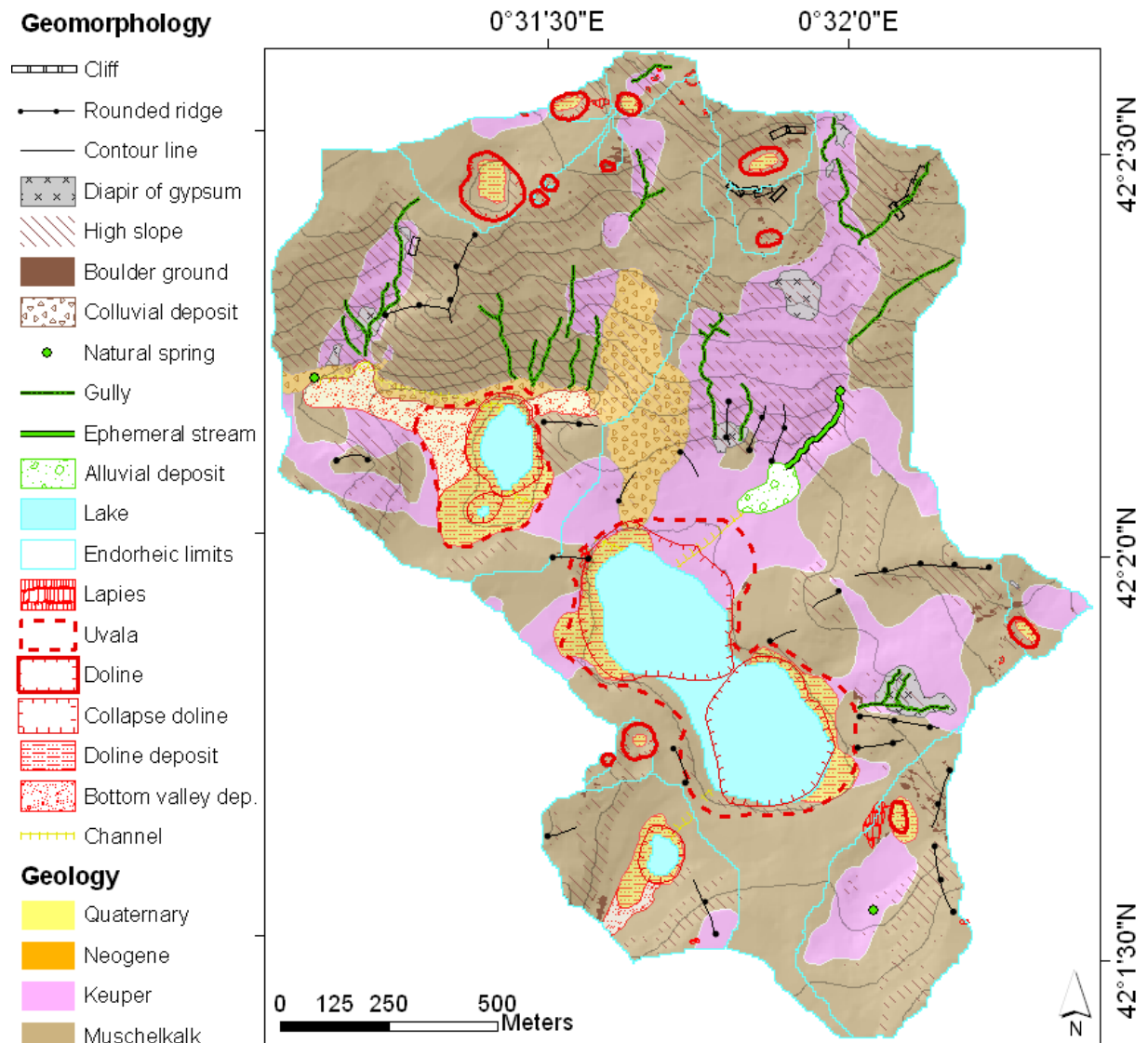
Fig. 7. Geomorphological map.

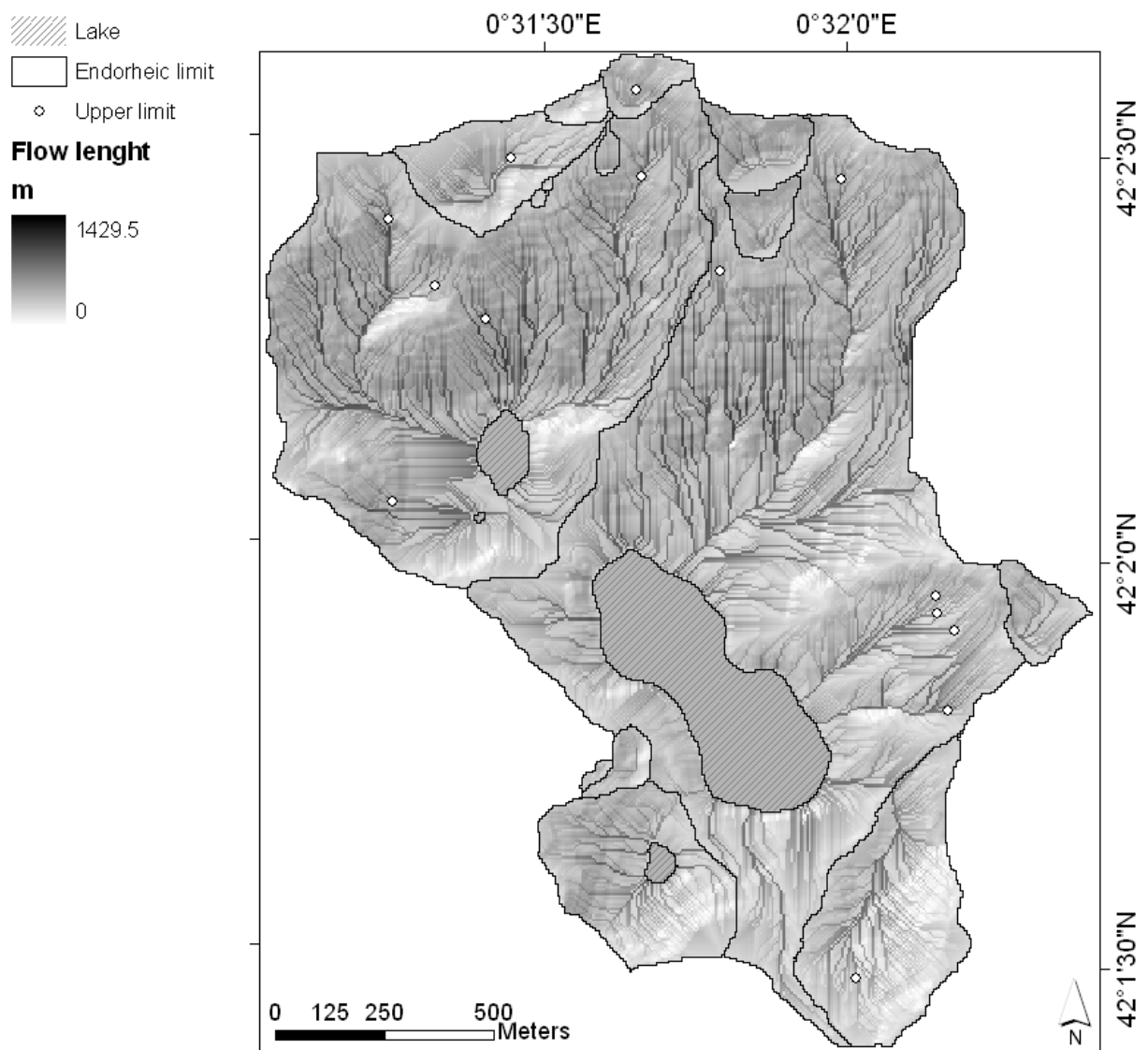**Fig. 8.** Upper limit points draped over the flow length map (downward from divides).

Fig. 9. Map of the LS-RUSLE factor.